

# RARE/Turbo Spin Echo Imaging with Simultaneous Multislice Wave-CAIPI

Borjan A. Gagoski,<sup>1,2†\*</sup> Berkin Bilgic,<sup>2,3†\*</sup> Cornelius Eichner,<sup>3,4</sup> Himanshu Bhat,<sup>5</sup> P. Ellen Grant,<sup>1,2</sup> Lawrence L. Wald,<sup>2,3,6</sup> and Kawin Setsompop<sup>2,3</sup>

**Purpose:** To enable highly accelerated RARE/Turbo Spin Echo (TSE) imaging using Simultaneous MultiSlice (SMS) Wave-CAIPI acquisition with reduced g-factor penalty.

**Methods:** SMS Wave-CAIPI incurs slice shifts across simultaneously excited slices while playing sinusoidal gradient waveforms during the readout of each encoding line. This results in an efficient k-space coverage that spreads aliasing in all three dimensions to fully harness the encoding power of coil sensitivities. The novel MultiPINS radiofrequency (RF) pulses dramatically reduce the power deposition of multiband (MB) refocusing pulse, thus allowing high MB factors within the Specific Absorption Rate (SAR) limit.

**Results:** Wave-CAIPI acquisition with MultiPINS permits whole brain coverage with 1 mm isotropic resolution in 70 s at effective MB factor 13, with maximum and average g-factor penalties of  $g_{\max} = 1.34$  and  $g_{\text{avg}} = 1.12$ , and without  $\sqrt{R}$  penalty. With blipped-CAIPI, the g-factor performance was degraded to  $g_{\max} = 3.24$  and  $g_{\text{avg}} = 1.42$ ; a 2.4-fold increase in  $g_{\max}$  relative to Wave-CAIPI. At this MB factor, the SAR of the MultiBand and PINS pulses are 4.2 and 1.9 times that of the MultiPINS pulse, while the peak RF power are 19.4 and 3.9 times higher.

**Conclusion:** Combination of the two technologies, Wave-CAIPI and MultiPINS pulse, enables highly accelerated RARE/TSE imaging with low SNR penalty at reduced SAR. **Magn Reson Med 000:000–000, 2015. © 2015 Wiley Periodicals, Inc.**

**Key words:** simultaneous multislice, multiband; Wave-CAIPI; MultiPINS; CAIPIRINHA; RARE/TSE/FSE

## INTRODUCTION

Rapid acquisition with refocusing echoes (RARE) (1), also known as turbo spin echo (TSE) or fast spin echo (FSE), is by far the most commonly used image readout sequence in clinical imaging. This versatile tool can be tailored to provide T1, T2, and proton density weighted acquisitions. It provides rapid imaging compared with conventional single-echo spin-echo by acquiring multiple phase encoding lines per repetition time (TR). Following a  $90^\circ$  excitation, multiple  $180^\circ$  radiofrequency (RF) pulses are used to continually refocus the transverse magnetization, thereby recording multiple spin echos. While this strategy permits efficient sampling of k-space, the application of large number of refocusing RF pulses results in increased power deposition to the target tissue. It is possible to mitigate this issue by simply reducing the flip angle of the refocusing pulses (2), or by fully refocusing the echo signals acquired at the center of k-space, and using lower flip angles to encode higher spatial frequencies (3).

RARE acquisition has been sped up though the use of in-plane parallel imaging, which undersamples two-dimensional (2D) k-space to reduce the number of phase encoding lines that needs to be acquired. However, at acceleration factor of 3 or above, the g-factor noise amplification in reconstructing this 2D undersampled acquisition and the  $\sqrt{R}$  noise penalty becomes too large. The RARE sequence can be further accelerated with the use of simultaneous multislice (SMS) imaging (4–9), wherein multiple slices are excited, refocused and read-out simultaneously. Such acquisition enables acceleration without reducing the number of k-space lines and hence without the  $\sqrt{R}$  penalty (9). Furthermore, SMS imaging has been shown to be amenable to controlled aliasing in two dimensions (y-z) by means of CAIPIRINHA technique, or CAIPI for short, to increase distance between aliased voxels and significantly reduce g-factor penalty. However, the application of SMS in RARE imaging further aggravates the specific absorption rate (SAR) issue because conventional multiband (MB) RF pulses are generated by means of superposition of single band sinc RF pulses, which makes the total deposited RF power proportional to the MB factor (10). A novel proposal termed power independent of number of slices (PINS) (11) creates a periodic excitation pattern obtained by undersampling of single-slice RF pulses. In contrast to conventional MB excitation, total power deposition of PINS is independent of the MB factor, thus making it particularly useful for ultra high field applications, slice accelerated spin echo functional MRI and diffusion

<sup>1</sup>Fetal-Neonatal Neuroimaging & Developmental Science Center, Boston Children's Hospital, Boston, Massachusetts, USA.

<sup>2</sup>Department of Radiology, Harvard Medical School, Boston, Massachusetts, USA.

<sup>3</sup>Athinoula A. Martinos Center for Biomedical Imaging, Massachusetts General Hospital, Charlestown, Massachusetts, USA.

<sup>4</sup>Max Planck Institute for Human Cognitive and Brain Sciences, Leipzig, Germany.

<sup>5</sup>Siemens Medical Solutions USA Inc., Charlestown, Massachusetts, USA.

<sup>6</sup>Harvard-MIT Health Sciences and Technology, Cambridge, Massachusetts, USA

Grant sponsor: NIH; Grant numbers: R00EB012107; P41RR14075; R01EB017337; Grant sponsor: NIH Blueprint for Neuroscience; Grant number: 1U01MH093765 (Human Connectome Project).

\*Correspondence to: Borjan A. Gagoski, PhD, 1 Autumn Street, AU457, Boston, MA, 02215. E-mail: borjan.gagoski@childrens.harvard.edu and Berkin Bilgic, PhD, Building 75, 13th Street, Charlestown, MA, 02129

Additional Supporting Information may be found in the online version of this article.

<sup>†</sup>Drs. Gagoski and Bilgic contributed equally to this work.

Received 10 October 2014; revised 21 December 2014; accepted 22 December 2014

DOI 10.1002/mrm.25615

Published online 00 Month 2014 in Wiley Online Library (wileyonlinelibrary.com).

© 2015 Wiley Periodicals, Inc.

imaging experiments (12,13). PINS pulses were also recently applied to the RARE sequence (14) to enable SMS-RARE imaging at 7T. This previous study used Blipped-CAIPI acquisition that creates interslice shifts across collapsed slices for improved parallel imaging (4,7), which yielded high quality images at an MB acceleration factor of 8 with 2 mm and 3 mm slice thickness.

In this contribution, we push the SMS acceleration even further to reach an MB factor of 15, thereby enabling whole brain RARE acquisition with an echo train length (ETL) of 12 and 1 mm isotropic resolution in 70 s. With this MB15 implementation, the coronal slice field of view (FOV) was set to 255 mm and because two of the excited slices in each slice group remain outside the head for our test subject, the effective MB factor ( $MB_{\text{eff}}$ ) in this case is 13. The two limiting factors that impede attaining such acceleration factors are (i) the increased power deposition needed for high quality PINS excitation and refocusing of thin slice imaging at short pulse duration of 5–6 ms required for efficient RARE imaging, and (ii) the substantial g-factor penalty that would be incurred by existing parallel imaging methods. We address both of these issues by using the novel MultiPINS (15) RF pulses that enable low SAR refocusing with Wave-CAIPI acquisition (16) that fully harnesses the spatial variation in coil sensitivity profiles to mitigate the g-factor penalty. The combination of the two technologies yield maximum and average g-factors of  $g_{\text{max}} = 1.34$  and  $g_{\text{avg}} = 1.12$  with a commercial 32-channel brain array while substantially reducing imaging at  $MB_{\text{eff}}=13$  under SAR safety constraint at 3T.

The specific contributions of this work are: (i) Using novel MultiPINS refocusing pulses to dramatically reduce the RF power deposition in RARE experiments, thus permitting high MB factors to be achieved in vivo within the SAR limit. (ii) Deploying Wave-CAIPI acquisition/reconstruction framework in SMS RARE imaging to achieve  $MB_{\text{eff}}$  factor 13 with reduced g-factor penalty. This enables a whole brain T2-weighted acquisition at 1 mm isotropic resolution in 70 s. (iii) Releasing supplementary Matlab code that replicates in vivo Wave-CAIPI and blipped-CAIPI reconstructions with  $MB_{\text{eff}}$  factor 13 at [martinos.org/~berkin/software](http://martinos.org/~berkin/software).

## METHODS

### MultiPINS: Low Power RF Pulse for SMS Excitation and Refocusing

Conventional SMS excitation involves MB pulses that are formed by the addition of multiple single-slice RF waveforms (17). The drawback of this superposition is the linear increase in transmitted energy and peak power deposition with the MB factor. Peak power of an MB pulse can be reduced through an optimized RF phase schedule (18) or a pulse time-shifting scheme (19), but these techniques do not reduce SAR. The VERSE algorithm (20) reduces both peak power and SAR, but can result in unacceptable slice-profile distortion and long pulse duration at high MB factors.

In contrast, PINS pulses (11) create a periodic excitation pattern obtained by undersampling of a single-slice

RF pulse, which makes the energy deposition independent of the number of excited slices. As the PINS pulses are divided into distinct time-bands containing RF sub-pulses to achieve such undersampling, fast traversal of excitation k-space becomes difficult. These pulses can be lengthy for thin slice imaging, leading to undesirably long echo-train length in RARE imaging and large off-resonance slice shift. PINS pulses can be shortened by reducing the sub-pulse duration, but this comes at the cost of increased SAR and peak RF power.

In MultiPINS (15), MB and PINS pulses are synergistically combined to reduce energy transmission and peak RF power, which also permits shorter pulses without exceeding SAR limits. We have demonstrated the efficacy of MultiPINS for high-resolution diffusion imaging at 7 Tesla (T), where SAR was reduced by 51% compared with PINS excitation (15). Herein, we demonstrate its efficacy for SMS-RARE imaging with 1mm slice thickness. While these MultiPINS are designed to excite 15 slices simultaneously within a slice FOV of 255 mm, the effective MB factor is 13 because two of the excited slices usually remain outside the head due to large FOV.

Because PINS sub-pulses are played only *between* the gradients blips, MultiPINS uses the time interval *during* the blips to play MB pulses. MultiPINS uses this strategy with an optimal mixing ratio of the two types of pulses, leading to reduced peak RF power and SAR specification. Figure 1 further demonstrates the application of MultiPINS to attain high SMS acceleration factor.

### Wave-CAIPI for Highly Accelerated SMS Imaging

CAIPIRINHA (abbreviated as CAIPI) controlled aliasing technique creates interslice shifts across simultaneously excited slices to improve unaliasing in SMS imaging (4). This is achieved by modulating the phase of the readout lines to create a phase ramp in k-space, which leads to a slice shift in the image space. Such modulation can be generated either by performing RF excitation with distinct phase cycling schemes across the different slices (4), or by playing  $G_z$  gradient blips that incur a phase ramp in  $z$  (slice) direction (7). CAIPI acquisition has been successfully deployed in volumetric (21), steady state free precession (SSFP) (22), diffusion (23), perfusion (24–26), and functional imaging (27). Clinical investigations of this strategy have demonstrated good image quality up to an acceleration factor of 4 in structural imaging (28,29). Acceleration factor of up to 8–9 had been shown (14), but such acquisitions suffer from g-factor penalty that can reduce SNR by as much as 30–40%, particularly in the central brain region where intrinsic SNR of the coil array is low (16).

Wave-CAIPI overcomes this issue by efficient sampling of k-space that spreads the aliasing evenly in all three dimensions to fully use the variation in the coil sensitivity profiles, thereby providing dramatic scan time reduction at negligible SNR and artifact penalties. We have previously deployed Wave-CAIPI in 3D-GRE imaging, and demonstrated that maximum g-factor  $g_{\text{max}}$  remains below 1.10 for R = nine-fold acceleration (16). Herein, we extend the Wave-CAIPI concept to multiband imaging using the SMS 3D k-space formalism (30).

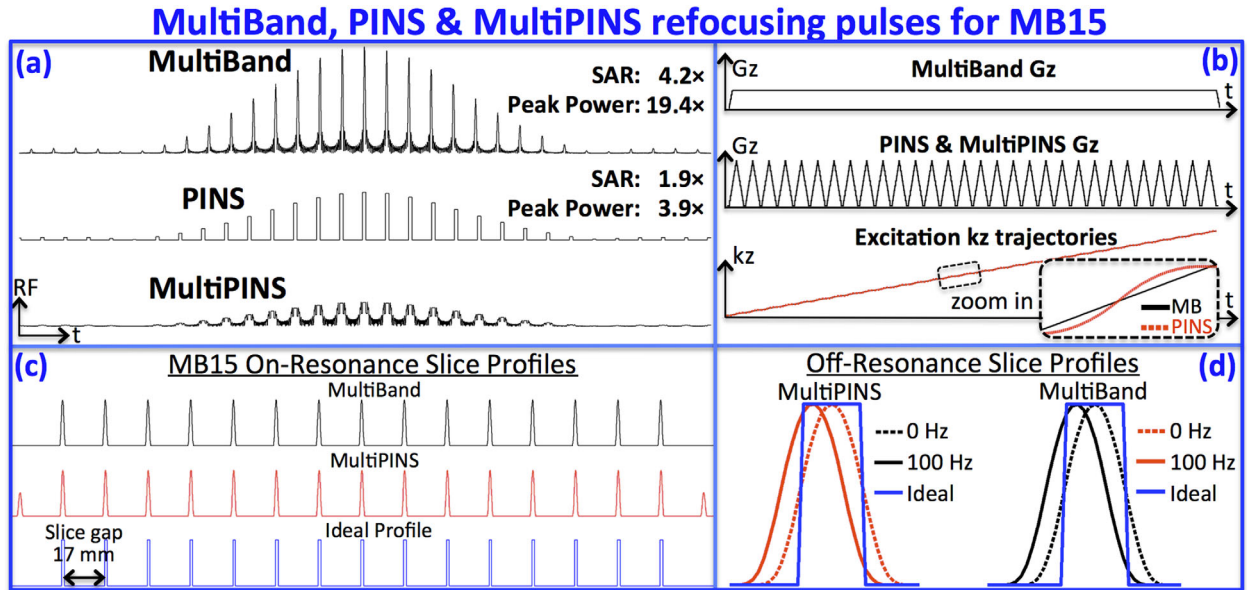


FIG. 1. Comparison of MultiBand, PINS and MultiPINS refocusing pulses at MB-15 and 1-mm slice thickness. **a**: Compared with MultiPINS, MultiBand and PINS designs have increased SAR and peak power deposition (4.2 $\times$  and 1.9 $\times$  SAR, and 19.4 $\times$  and 3.9 $\times$  peak power in this example). **b**: Gradient waveforms and excitation  $k$ -space trajectories for MultiBand and MultiPINS. Despite differences in the gradient waveforms, the  $k$ -space traversals are very similar; minor deviations from linear transversal of MultiPINS are shown in the zoomed panel. As such, MultiPINS exhibits good off-resonance performance with negligible slice distortion. **c**: Similar refocusing profiles of MultiBand and MultiPINS, with additional sidelobes outside the volume of interest for MultiPINS from the PINS component of the pulse. **d**: Zoomed in comparison of profiles at 0 and 100 Hz. The profile at 100 Hz contains a simple shift essentially identical to MultiBand profile at the same frequency. No slice profile distortions can be observed.

It is possible to represent SMS imaging as undersampling in 3D  $k$ -space (30,31) by relying on the fact that alternating gradient blips (or phase of RF pulses) conduct Discrete Fourier Transform (DFT) along the slice axis. Recognizing the distance between the simultaneously excited slices  $\Delta z$  (i.e., slice separation) as the inherent slice resolution, the  $k$ -space sampling period  $\Delta k_z$  needs to be  $1/(N \cdot \Delta z)$  to fully sample the  $N$  slices. In the presence of field-of-view (FOV) shifting in the phase encoding direction by an amount  $FOV/L$ , the blipped-CAIPI sampling period becomes  $\Delta k_z^{\text{blip}} = 1/(L \cdot \Delta z)$ , thus effectively undersampling the SMS 3D  $k$ -space. The staggered  $k$ -space sampling pattern that gives rise to slice shifting is demonstrated in Figure 2a for MB factor 15 ( $N=15$ ), with  $FOV/4$  shift ( $L=4$ ). We note that the CAIPIRINHA method, which uses RF phase modulation, also creates the same  $k$ -space shift as the blipped-CAIPI method.

The effect of playing the sinusoidal Wave gradients during the readout period of each RARE/TSE phase encoding line is to create a helical  $k$ -space trajectory that increases the coverage in the undersampled SMS 3D  $k$ -space. When the centers of each helix is staggered in the blipped-CAIPI manner, the resulting trajectory spreads the undersampling to all three  $k$ -space axes, rather than fully sampling the readout dimension and sparsely sampling the  $k_y$ - $k_z$  plane (Fig. 2b). This allows Wave-CAIPI to use all degrees of freedom in the coil sensitivity maps and improve the  $g$ -factor. If we look at this trajectory in the  $k_y$ - $k_z$  plane by fixing a particular  $k_x$  position, the relative position of each sample will be identical to that of blipped-CAIPI sampling, meaning that the helical trajectory of each  $k_x$  readout line does not intersect with the other  $k_x$  lines in

the Wave-CAIPI acquisition. Wave-CAIPI builds upon the Bunched Phase Encoding (BPE) (32) and zigzag sampling strategies (33,34) to improve the  $k$ -space coverage along phase encoded dimensions by oversampling in the readout direction. A similar strategy has also been applied to GRASE (gradient and spin echo) imaging (35,36), wherein zigzag sampling allowed distribution of T2 modulations and off-resonance effects to different axes (vGRASE) (37). These methods, however, require either gridding or multiple GRAPPA (38) kernels for reconstruction.

As further demonstrated in Figure 2b, the non-Cartesian trajectory in Wave-CAIPI acquisition can be expressed as convolution in Cartesian space, thereby obviating the need for gridding or nonuniform Fourier Transform. As detailed in Bilgic et al (16), each readout line is convolved with a different point spread function (PSF) to create different amount of voxel spreading as a function of space. Note that the spreading effect is only along the readout ( $x$ ) direction, with the amount of spreading varies based on the ( $y$ ,  $z$ ) coordinate of the voxels. Combined with interslice FOV shifts, the sinusoidal Wave gradients create highly spread-out data in image space. This increases the average distance between collapsed voxels in the SMS acquisition and substantially improves the parallel imaging capability.

#### Characterization of Off-Resonance Effects for Wave-CAIPI

Wave-CAIPI provides a rapid acquisition without undesirable image distortion/blurring from B0 inhomogeneity. This is because Wave-CAIPI traverses  $k$ -space in the readout direction with the same constant rate as conventional acquisitions, with B0 inhomogeneity-related phase

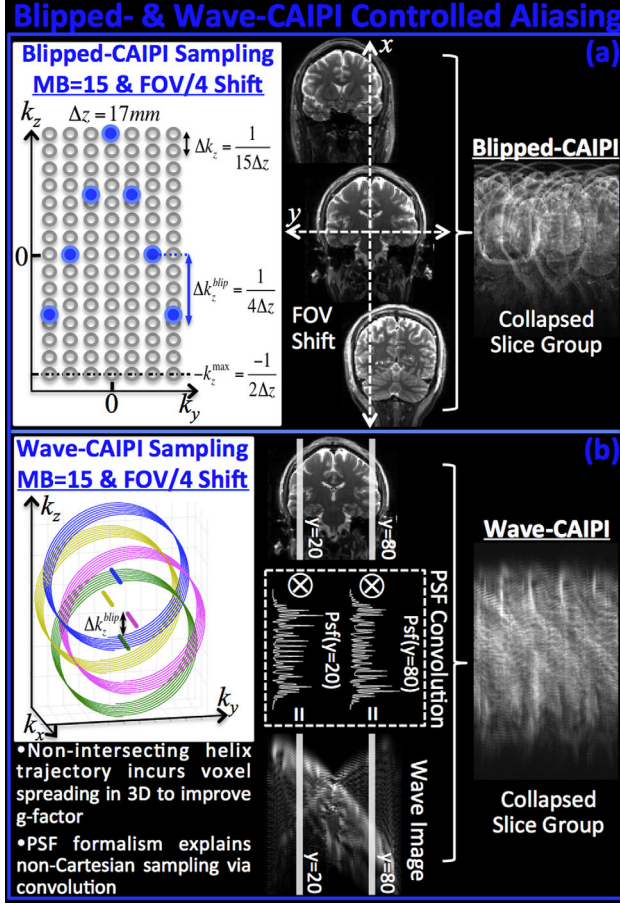


FIG. 2. K-space and image space view of controlled aliasing with Blipped- and Wave-CAIPI. **a**: Blipped-CAIPI SMS imaging can be reformulated as undersampling in 3D  $k$ -space with staggered sampling, which induces slice shifts in the phase encoding direction. **b**: Wave-CAIPI traverses a helical trajectory that distributes the undersampling to all  $k$ -space axes along with staggered sampling of PE. The helical trajectory incurs voxel spreading in image space in the readout direction that increases the average distance across collapsed voxels, thus improving  $g$ -factor substantially. Non-Cartesian Wave trajectory can be represented as convolution with a spatially varying point spread function that permits Cartesian reconstruction.

evolving solely as a function of  $k_x$ . To validate this, a water phantom was scanned at 3T using conventional and Wave-CAIPI 3D-GRE sequences with 2 mm isotropic resolution,  $96 \times 96 \times 60$  matrix size,  $\text{FOV} = 192 \times 192 \times 120$ ,  $\text{TR}/\text{TE} = 20/10$  ms and 100 Hz/pixel bandwidth. Both datasets were fully sampled and acquired in the presence of large  $B_0$  off-resonance (500 Hz) imposed by manually offsetting the  $B_0$  shims. To serve as ground truth, normal GRE data were also collected on-resonance with otherwise identical parameters.  $B_0$  mapping was conducted using three sequentially acquired normal GRE volumes with echo times  $\text{TE}_1/\text{TE}_2/\text{TE}_3 = 9.5/10/10.5$  ms.

#### Data Acquisition and Reconstruction

RARE/TSE sequence was modified to include sinusoidal  $G_y$  and  $G_z$  gradient modules as well as gradient blips that create interslice shifts used in Wave-CAIPI trajectories. The pulse sequence diagram including the  $90^\circ$  MB and

$180^\circ$  MultiPINS pulses is depicted in Figure 3, where the echo train length (ETL) is set to 2 for display purposes.

A healthy subject (male, age 33) was imaged on Siemens Tim Trio 3T system in accordance with the institutional review board protocol to acquire MB-15 RARE/TSE data with 1 mm isotropic resolution. The effective MB factor,  $\text{MB}_{\text{eff}}$ , was 13 because two slices in each slice group remained outside the head. For signal reception, 32-channel Siemens head coil was used. The bandwidth was chosen to be similar to the protocol in Norris et al (14), and was set to 130 Hz/pixel and  $\text{ETL} = 12$ . The in-plane matrix size was  $256 \times 192$  with 255 coronal slices, and the repetition (TR) and echo times (TE) were  $\text{TR}/\text{TE} = 4000/90$  ms with an echo spacing of 18 ms. Using the same parameter setting, Blipped-CAIPI and Wave-CAIPI data were acquired within an acquisition time of  $T_{\text{acq}} = 70$  s. Because SMS imaging excites multiple slices simultaneously and records them for the same duration in an unaccelerated 2D scan (9), it does not incur the intrinsic  $\sqrt{R}$  SNR penalty that occurs when the time window of signal accumulation is reduced. The SNR advantage of eliminating the  $\sqrt{R}$  penalty is particularly significant at high acceleration: the  $\sqrt{R}$  penalty alone would have led to a  $\sim 3.9$ -fold drop in SNR for 15-fold in-plane acceleration. As such, the present study used SMS acceleration only.

For comparison, MB-1, fully sampled, product RARE/TSE data were acquired. Owing to the stepwise increments in the echo time, TE was set to 84 ms, while the echo spacing was 16.8 ms. Only 14 slices could be acquired within the same acquisition time of 70 s. All other parameters were identical to the Blipped- and Wave-CAIPI acquisitions. The Wave PSFs used in slice unaliasing reconstruction were determined using the  $k$ -space trajectory estimation scheme in Bilgic et al (16). For the PSF calibration, data were acquired on a phantom before the in vivo acquisition.

Coil sensitivity profiles were estimated using low-resolution ( $2 \times 2 \times 3 \text{ mm}^3$ ) TSE data, and were iteratively refined using J-SENSE algorithm (39) with 7<sup>th</sup> order polynomial fitting for smoothing. As presented in the flowchart in Supporting Figure S1, which is available online, estimated PSFs and coil sensitivities are used in generalized SENSE reconstruction (40,41) to unalias simultaneously excited slices in the Wave-CAIPI acquisition.

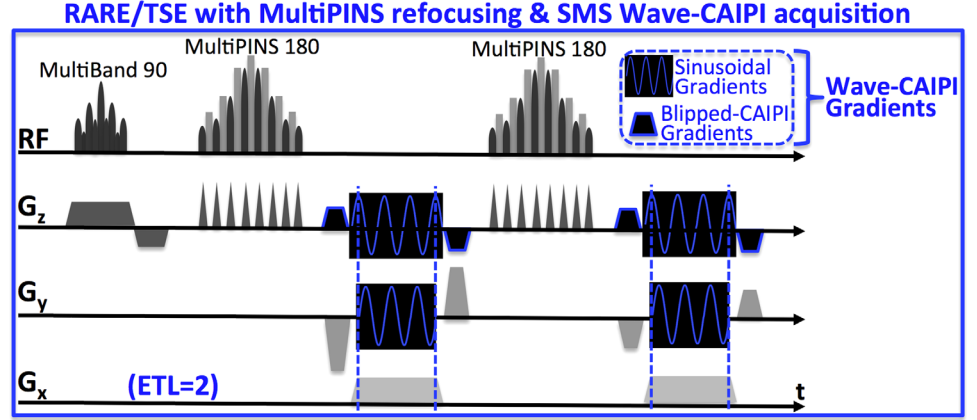
#### $g$ -Factor Map Computation

Follows the  $g$ -factor formulation for SENSE reconstruction outlined in Pruessmann et al (40), and has been modified it to incorporate the Wave point spread functions. Specifically, Wave-CAIPI decouples the reconstruction into subproblems that are solved independently for each set of collapsed readout rows. At MB15, we solve for one readout row from 15 slices at a time, and loop over phase encoding positions and slice groups. This leads to the generalized SENSE model,

$$\begin{bmatrix} W_1 C_{11} S_1 & \dots & W_N C_{1N} S_N \\ \vdots & \vdots & \vdots \\ W_1 C_{M1} S_1 & \dots & W_N C_{MN} S_N \end{bmatrix} \begin{bmatrix} \text{slice}_1 \\ \vdots \\ \text{slice}_N \end{bmatrix} = \begin{bmatrix} \text{coil}_1 \\ \vdots \\ \text{coil}_M \end{bmatrix} \quad [1]$$

where  $\{\text{slice}_j\}_{j=1}^N$  are the readout rows from each slice within the collapsed slice group,  $\{\text{coil}_i\}_{i=1}^M$  are the

FIG. 3. RARE/TSE pulse sequence diagram for echo train length 2 (ETL=2). Blipped- and Wave-CAIPI gradient modules are inserted in  $G_y$  and  $G_z$  axes to provide controlled aliasing, while MultiPINS RF pulses permit low SAR refocusing.



collapsed coil images,  $\{S_j\}_{j=1}^N$  are the slice-shifting operators that undo the blipped-CAIPI interslice shifts,  $\{W_j\}_{j=1}^N$  are the Wave point spread operators, and  $C_{ij}$  are the coil sensitivities. To capture the noise correlation across the receive channels, the coil sensitivities and the coil images are prewhitened with the inverse square root of the covariance matrix,  $\Psi^{-1/2}$ . For the current experiments, RF pulses are designed to excite  $N=15$  slices simultaneously and  $M=32$  coils are used for reception. Compactly representing this system as  $\mathbf{E} \cdot \text{slice} = \text{coil}$  the g-factor value at position  $r$  can be evaluated in closed-form as  $g_r = \sqrt{[(\mathbf{E}^H \mathbf{E})^{-1}]_{rr} (\mathbf{E}^H \mathbf{E})_{rr}}$ .

Image reconstruction for all experiments was performed in Matlab running on a workstation with 128GB memory and 32 AMD Opteron CPU processors.

#### Effect of Magnetization Transfer Contrast (MTC)

To investigate the MTC effect of the MB-15 MultiPINS refocusing pulses, a healthy volunteer (female, age 26) was imaged at 3T with the same whole-brain Wave-CAIPI acquisition protocol (1 mm isotropic voxels, 255 slices, TR/TE=4000/90 ms). Two additional Wave-CAIPI volumes were also collected at TE=72 and 126 ms, with otherwise same parameters. For comparison, fully

sampled, MB-1 product RARE/TSE sequence with the same in-plane resolution and TR/TE=4000/84 ms was used to acquire multislice (14 slices) and single-slice datasets.

## RESULTS

Figure 1a shows MultiBand, PINS, and MultiPINS RF refocusing pulses for MB-15 RARE/TSE imaging, with pulse duration of 6 ms and time-bandwidth product of 2.4, on the same order as in single slice RF in clinical RARE imaging. In this example, the SAR of the MultiBand and PINS pulses are 4.2 and 1.9 times that of the MultiPINS pulse, while the peak power (proportional to square of maximum voltage) were 19.4 and 3.9 times higher. The MultiPINS pulse was the only one that could be used for in vivo MB-15 SMS-RARE imaging without exceeding the SAR limit (results in Figures 5 and 6). Figure 1b shows gradient waveforms for MultiBand and MultiPINS designs, and corresponding k-space trajectory as a function of time. Despite marked differences of the gradient waveforms, the k-space traversals are very similar—minor deviations from linear transversal of MultiPINS are shown in the zoomed panel. As such, MultiPINS exhibits good off-resonance performance with negligible slice distortion. Figure 1c shows the on-resonance refocusing profiles of MultiBand, MultiPINS,

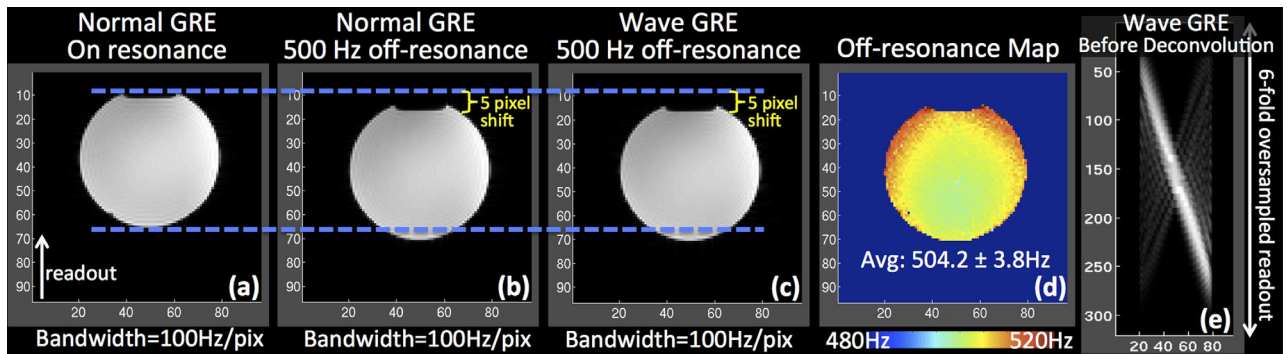


FIG. 4. The effect of off-resonance on Wave-CAIPI acquisition is a voxel shift in the readout direction identical to conventional acquisition. **a**: Normal GRE data acquired on-resonance. **b**: Normal GRE acquired at 500 Hz off-resonance. **c**: GRE acquired using Wave-CAIPI trajectory at 500 Hz off-resonance. **d**: Estimated  $B_0$  map. **e**: Wave-CAIPI image before deconvolution with point spread functions.

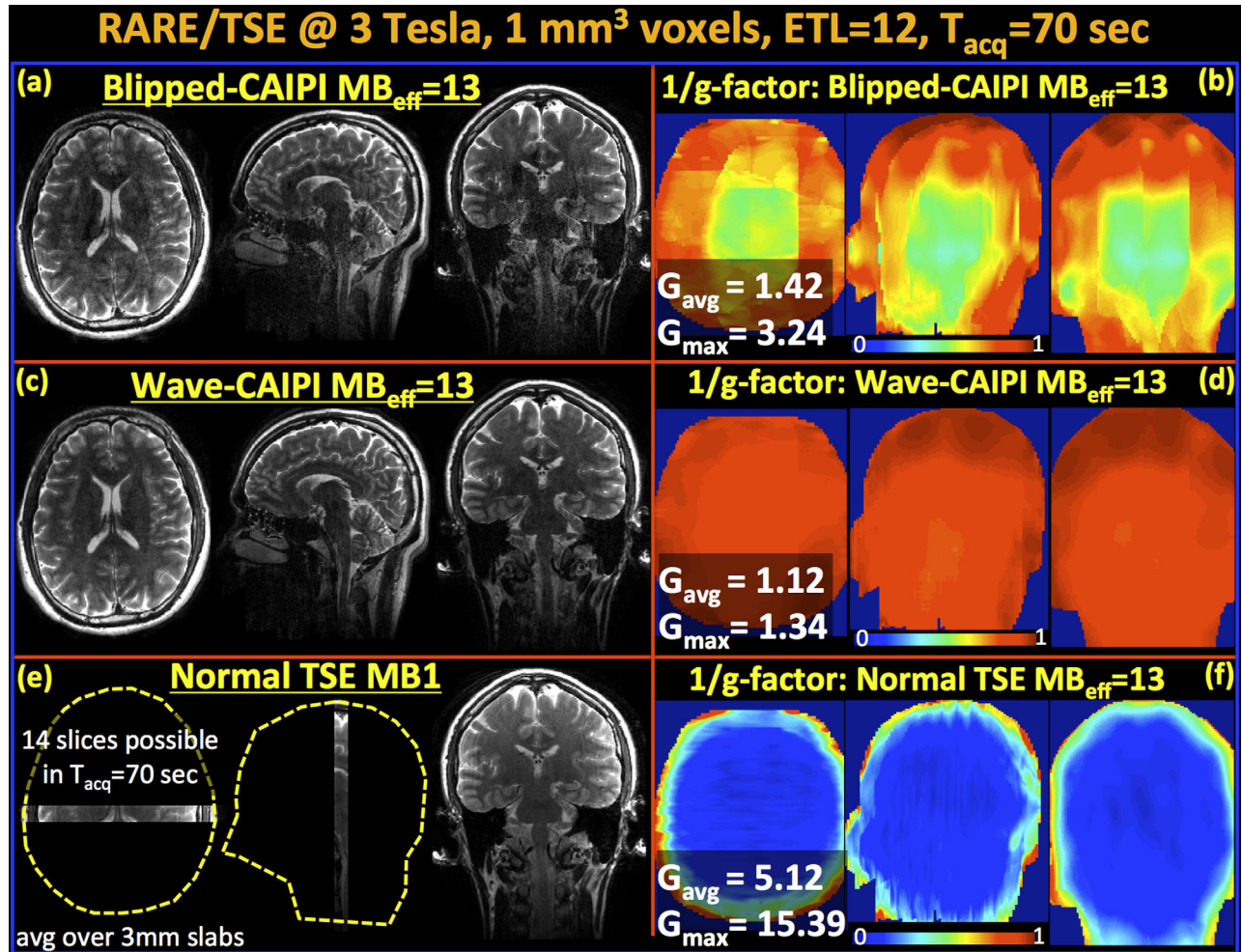


FIG. 5. Reconstructed volumes and  $g$ -factor analysis for MB-15 RARE/TSE at 3T. Because two slices remain outside the head, this leads to an effective MB factor of  $MB_{\text{eff}} = 13$ . **a, b**: Blipped-CAIPI suffers from noise amplification especially in middle of the volume with  $g_{\text{max}} = 3.24$  and  $g_{\text{avg}} = 1.42$ . **c, d**: Wave-CAIPI yields high quality data and close to perfect SNR retention with  $g_{\text{max}} = 1.34$  and  $g_{\text{avg}} = 1.12$ . **e**: Fully sampled MB-1 product RARE/TSE acquisition is able to cover a very limited FOV (14 slices) in the same acquisition window. **f**: The  $1/g$ -factor analysis for  $MB_{\text{eff}} = 13$  reconstruction *without* FOV shifting and Wave. All images (a, c, e) are scaled identically.

and ideal excitation, while Figure 1d presents a zoomed in comparison of profiles at 0 and 100 Hz. The profile at 100 Hz contains mostly a simple shift essentially identical to MultiBand's profile at the same frequency (correlation coeff.  $> 0.99$ ). The slice profile also shows partial refocusing outside the volume of interest resulting from the PINS component of the MultiPINS pulse. This would affect axial imaging, but can be overcome using a MB excitation before MultiPINS refocusing, similar to what we have demonstrated for PINS diffusion imaging (15).

The effect of off-resonance acquisition for Wave-CAIPI is demonstrated in Figure 4, where the Wave-CAIPI reconstruction results in a sharp image with the same image shift of five voxels along the readout direction as the standard acquisition.

Parallel imaging reconstruction and  $g$ -factor analysis results for Wave- and blipped-CAIPI are shown in Figures 5a–d. The maximum  $g$ -factors over the whole volume were  $g_{\text{max}} = 1.34$  and  $3.24$ , while the average  $g$ -factors were  $g_{\text{avg}} = 1.12$  and  $1.42$  for blipped- and Wave-CAIPI imaging at  $MB_{\text{eff}} = 13$ . Wave-CAIPI is seen to retain

SNR and image quality more successfully than blipped-CAIPI acquisition, especially in the middle of the imaging volume where the receive coils have decreased sensitivity and are less orthogonal to each other—leading to increased  $g$ -factor penalty in such region (42,43) (Figs. 5b and d). Figure 5e shows the images from fully sampled, product MB-1 RARE/TSE protocol that allowed acquisition of only 14 slices in the same imaging time of 70 s, thus being able to cover a very limited FOV. All images are averaged over a 3-mm slab to mimic standard clinical RARE imaging with thick slices that are familiar to the radiologists, but now with the ability for multi-orientation formatting. Additionally, Figure 5f shows the  $1/g$ -factor maps that would have been obtained if  $MB_{\text{eff}} = 13$  imaging was applied *without* FOV shifting or Wave gradients. In this case, the maximum and average  $g$ -factors would have been  $g_{\text{max}} = 15.39$  and  $g_{\text{avg}} = 5.12$ , leading to unacceptable level of SNR loss.

Figure 6 shows unaliased slices from a collapsed slice group for blipped- and Wave-CAIPI reconstruction. When the slices outside of the brain were excluded, the

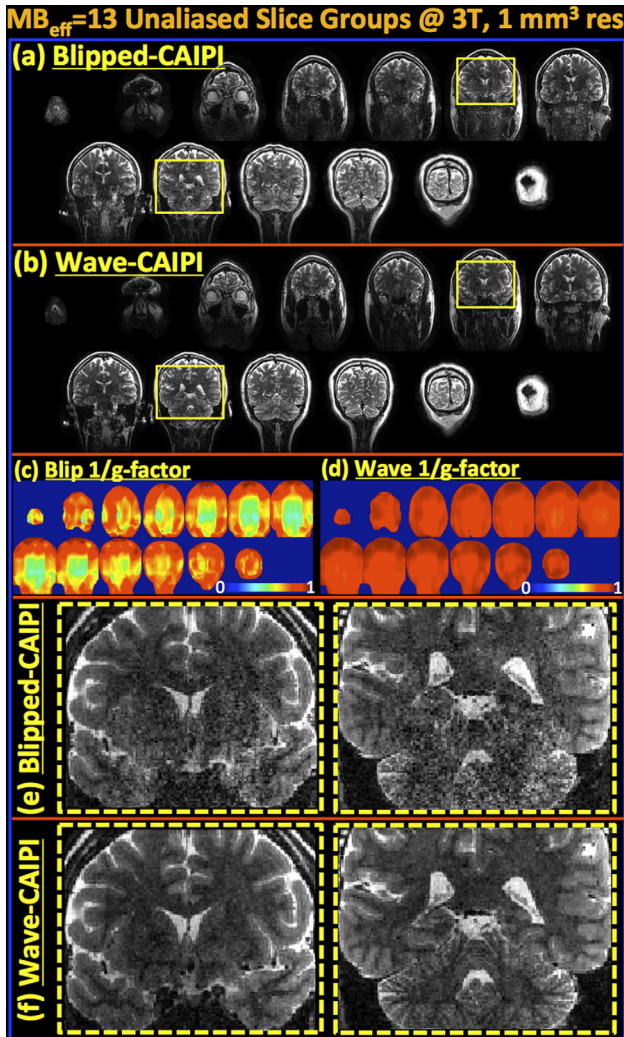


FIG. 6. Unaliased slices from a representative single group of 13 collapsed slices are compared for blipped- (a) and Wave-CAIPI (b) acquisition. c,d: Depict corresponding  $1/g$ -factor maps for the slice groups. e,f: Two slices are further magnified to demonstrate the improvement in SNR retention provided by Wave-CAIPI relative to blipped-CAIPI.

effective number of aliased slices were 13 for the MB-15 acquisition. Two of the slices are further zoomed in to show the improvement in SNR and reduced image artifact with Wave-CAIPI imaging.

Wave-CAIPI reconstruction time for the 1 mm isotropic whole-brain dataset was 63 min, while this was 2.2 min for Blipped-CAIPI. Coil sensitivity estimation with JSENSE required 5.4 min of computation with 10 iterations.

## DISCUSSION

This contribution addresses the two impeding factors that prevent ultra fast SMS-RARE/TSE imaging, namely SAR limitation and  $g$ -factor penalty. As RARE imaging involves multiple  $180^\circ$  refocusing pulses per  $90^\circ$  excitation, energy deposition is a main limitation to the number of slices that can be simultaneously excited. By using the novel MultiPINS RF excitation pulses, we remove this restriction and achieve  $MB_{\text{eff}}$  factor 13 by

dramatically reducing the incurred SAR and peak power. While controlled aliasing with CAIPI is shown to provide high quality images at up to four-fold acceleration (28,29), it fails to attain higher acceleration factors without significant penalty to SNR and artifact level. Higher acceleration factors of 8–9 using CAIPI slice shifting have been demonstrated (14,16), but such speed up comes at the cost of elevated  $g$ -factor, which can reach up to  $g_{\text{max}} = 1.8$  in the central brain region. We deploy the novel Wave-CAIPI acquisition to SMS imaging and substantially mitigate the  $g$ -factor and image artifact penalty to provide whole-brain RARE/TSE with 1 mm isotropic resolution in 70 s. For Wave-CAIPI SMS acquisitions, the combination of (i) acceleration by acquiring more slices rather than undersampling  $k$ -space (thus avoiding the  $\sqrt{R}$  penalty) and (ii) an effective strategy to spread aliasing to minimize  $g$ -factor is very powerful. To put things in perspective, the total SNR penalty in  $15\times$  SMS  $T_2w$ -RARE with Wave-CAIPI ( $g_{\text{max}} = 1.34$ ) is lower than the  $\sqrt{R}$  penalty component of 2D  $T_2w$ -RARE at  $R=2$  ( $\sqrt{R} = 1.41$ ) that is routinely used in clinical imaging.

With limited ability to spatially encode in the short time frame needed to be robust against motion, clinical imaging routinely uses 2D slice-by-slice acquisitions with high in-plane resolution and thick imaging slices at 20–30% slice-gap. This is undesirable because the gaps can cause small abnormalities to be missed while thick imaging slice necessitates imaging at multiple orientations to create high resolution data across multiple viewing planes, which lengthen scan time. An order of magnitude improvement in MRI acquisition efficiency is needed to enable inefficient and compromised multi-orientation 2D clinical imaging to be effectively replaced by SNR efficient SMS and 3D imaging at uncompromised sub-millimeter isotropic resolution. To this end, we aim to deploy the Wave-CAIPI acquisition across the important clinical sequences to enable a comprehensive, ultra fast, motion insensitive multicontrast protocol. We have taken concrete steps in this direction first with  $R=3 \times 3$ -fold accelerated 3D-GRE (16), and currently with  $MB_{\text{eff}}=13$  RARE/TSE. We will next target highly accelerated MPRAGE (44) and FLAIR (45) sequences to complement our rapid clinical protocol. Such multicontrast protocol consisting of SMS and 3D sequences will yield high-resolution images at isotropic resolution to provide more detailed information rapidly. Such information can also be reformatted into multiple viewing planes, thus obviating the need for lengthy acquisitions at multiple different image orientations.

It is crucial to provide high acceleration while preserving image contrast properties that are important for clinical diagnosis. For standard  $T_2w$ -RARE, an acquisition with a long TR is needed to create suitable  $T_2$  contrast. With MB-15, a long TR can be achieved through coronal-orientation imaging, where a large number of imaging slices is needed to fully cover the long axis of the brain (anterior–posterior). This enables high-MB acceleration while having a large number of slice-groups to effectively fill out the long TR (the example, Figures 5 and 6 have 255 slices with a 17 slice-group at MB-15, enabling effective RARE acquisition at TR of 4 s). SMS RARE/TSE

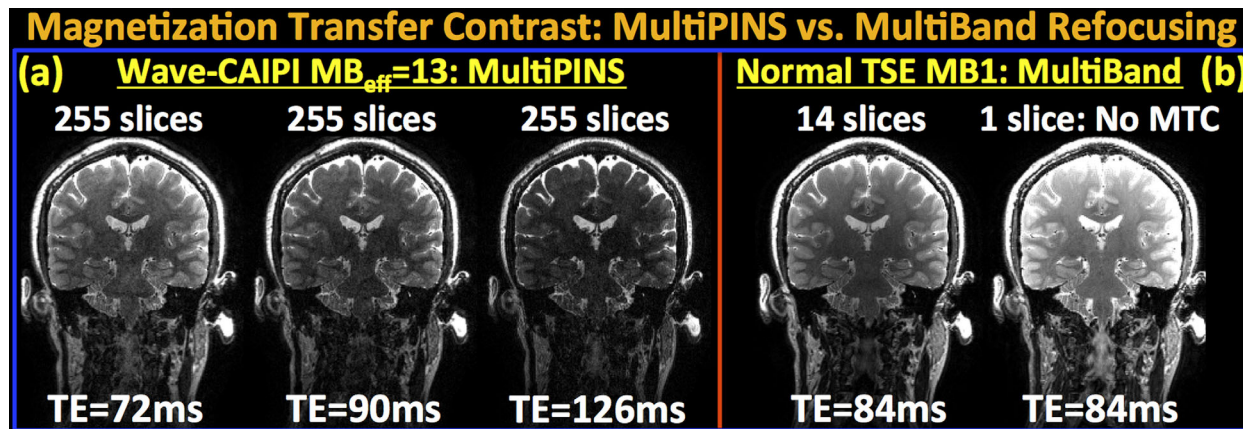


FIG. 7. Comparison of Magnetization Transfer Contrast (MTC) in MultiPINS and MultiBand refocusing. **a:** Wave-CAIPI reconstructions at  $MB_{\text{eff}} = 13$  with 255 slices at three different echo times,  $TE = 72, 90,$  and  $126$  ms. **b:** Product RARE/TSE at MB-1 with multi- and single-slice acquisitions at  $TE = 84$  ms. The 14-slice MB-1 images demonstrate reduced signal intensity relative to the single-slice acquisition due to the MT effect. Wave-CAIPI with MultiPINS refocusing has further increased MTC due to (i) increased number of slices (255 versus 14) contributing to MTC, and (ii) high bandwidth PINS sub-pulses that produce off-resonance excitation. To obtain contrast similar to the MB-1 product sequence,  $MB_{\text{eff}} = 13$  acquisition at the lower of  $TE = 72$  ms can be used.

imaging can be further accelerated by using in-plane undersampling. While  $R$ -fold in-plane acceleration will incur  $\sqrt{R}$  penalty to the SNR of the reconstructed images, such strategy can be beneficial for speed-up beyond MB-15 without reducing the TR necessary for T2-weighted contrast. In-plane acceleration will decrease the number of shots necessary to cover the  $k$ -space while retaining the long TR, thus will allow scan time reduction without introducing undesirable T1 contrast. In particular, Wave-CAIPI acquisition can be modified for synergistic combination with recent developments in multichannel compressed sensing using pseudorandom sampling (46–49).

For the comparisons in Figure 1, all refocusing pulses were of the same time-bandwidth product of 2.4 and also of the same pulse duration. However, as with actual acquisitions in this work, the Bloch simulation uses a 1-mm-thick  $90^\circ$  MB excitation pulse and a 1.3-mm-thick  $180^\circ$  refocusing pulse to provide an overall 1 mm profile as shown in Figure 1. As demonstrated by the Bloch simulation, the use of thicker slice profile for the  $180^\circ$  refocusing at  $1.3\times$  thickness still provides a good slice profile at 1 mm, because the overall profile has already been defined by the  $90^\circ$  excitation. Furthermore, because interleaved acquisition is used and TR is long, this thicker refocusing pulse will have minimal effect on the steady state signal level. Alternatively, a  $180^\circ$  refocusing pulse with 1 mm thickness can also be used, resulting in a time-bandwidth product of 1.8, which would still provide a relatively good refocusing profile.

As detailed in Bilgic et al (16), the non-Cartesian trajectory traversed by the sinusoidal Wave gradients can be captured in PSF formalism, which allows reconstruction with simple fast Fourier transforms (FFTs) and decoupled SENSE model. Additionally non-Cartesian, Wave-CAIPI trajectory does not sustain  $B_0$ -distortion that is encountered in, e.g., EPI or spiral acquisitions. As shown in Figure 4, Wave trajectory incurs the same amount of voxel shift in the readout direction due to  $B_0$  inhomogeneity, as would any Cartesian acquisition, with no additional blurring. As demonstrated in Figure 2b,

the radius of the Wave trajectory used in this work is even larger than the Blipped-CAIPI sampling period  $\Delta k_z^{\text{blip}}$ . As the radius grows larger, the voxel spreading amount in image space also rises, thus further increasing the average distance between collapsed voxels and the  $g$ -factor performance.

Clinical multislice  $T_2w$ -RARE imaging contains significant Magnetization Transfer Contrast (MTC) from the slice-selective RF pulses (50,51), which is substantially reduced in SMS  $T_2w$ -RARE imaging with PINS RF pulses (14). The optimal mixing ratio of MultiBand and PINS refocusing pulses used in the MB-15 MultiPINS designed to minimize SAR was 50%, leading to substantially reduced peak RF power and SAR. The flexibility of MultiPINS refocusing to combine MultiBand and PINS pulses at different ratios can be used to adjust the MTC as required for a specific clinical application, albeit at the cost of operating at sub-optimal peak power and SAR specifications. Figure 7 investigates the MTC contrast in MultiPINS refocusing by comparing the MB-15 reconstructions at different echo times with multi- and single-slice product RARE/TSE datasets at MB-1. As expected, MT effect reduces the signal level in the 14-slice MB-1 experiment relative to the single-slice acquisition that does not exhibit MTC. Using MB-15 MultiPINS pulses is seen to further amplify the MT effect due to the combination of two factors:

(i) Because the linewidth of the macromolecules that contribute to MTC extends over a large frequency range (1 kHz to 100 kHz) (2), even the RF pulses exciting much further slices contribute to the magnetization of the slice of interest (3). As the MD component of the MB-15 MultiPINS refocusing pulse excites substantially more slices compared with the time-matched MB-1 product sequence (255 versus 14 slices), the MT effect is more pronounced.

(ii) The sub-pulses used in the PINS component of the current MultiPINS design have a sub-pulse duration of 33  $\mu\text{s}$ , leading to a  $\pm 33$  kHz off-resonance bandwidth. This is much shorter than the sub-pulse durations of

PINS pulses in Breuer et al (4) which are designed for excitation and refocusing of thicker (2 and 3 mm) slices. Therefore, the current PINS design possess a much wider bandwidth, within which MT effects become significant.

The combined effect of (i) and (ii) leads to increased MTC in the Wave-CAIPI experiment, for which reducing the echo time is seen to provide similar contrast to the MB-1 multislice product acquisition. Specifically, MB-15 acquisition with  $TE = 72$  ms yields similar contrast to MB-1 product TSE at the longer echo time of  $TE = 84$  ms.

In this work, we have been able to take advantage of the relatively low bandwidth of the  $G_x$  readout gradient that is typically used in standard acquisitions to enable additional encoding through the corkscrew trajectory. For this, we have chosen to use mild  $G_y$ ,  $G_z$  sinusoidal waveforms, with low demand on maximum gradient amplitude and slew rate at 6 mT/m and 35 mT/m/s, to provide large additional k-space coverage as shown in Figure 2, which has proven to be adequate for good parallel imaging performance at MB-15 acceleration. Such sinusoidal gradients do not push the gradient system hardware to the limit and high fidelity gradients waveforms are created.

#### Limitations and Drawbacks

As outlined in the flowchart in Supporting Figure 1, Wave-CAIPI uses generalized SENSE reconstruction (41) and relies on coil sensitivity and PSF estimates for the forward data acquisition model. Because the PSFs depend only on the gradient hardware of the system, they need to be estimated once and can be used in successive acquisitions. As such, the current work used PSFs estimated on a phantom scanned before the in vivo acquisition, thus incurring no additional scan time. Receiver sensitivities, however, need to be estimated for each individual subject due to changes in the coil loading based on the interaction between the receivers and the subject. This work used lower resolution ( $2 \times 2 \times 3 \text{ mm}^3$ ) fully sampled RARE/TSE data to estimate the coil sensitivities, but a much more efficient 3D-FLASH (52) calibration acquisition can also be used such as outlined in Norris et al (14). Such acquisition, which is considerably faster, will also reduce the mismatch between the coil sensitivities and the SMS RARE/TSE data due to potential subject motion between the scans. Furthermore, automatic coil sensitivity estimation with ESPIRiT (53) might be a viable substitute for JSENSE, as it obviates the need for polynomial fitting for smoothing, and thus the dependency of sensitivities on the polynomial order. Using recent sensitivity estimation techniques such as (54,55) may also provide high-fidelity coil profiles.

As the Wave-CAIPI technique entails a more involved reconstruction step, it is computationally more expensive than blipped-CAIPI. Without the use of parallel computing, the Wave-CAIPI reconstruction time for the 1 mm isotropic whole-brain dataset was 63 min, whereas this was 2.2 min for Blipped-CAIPI. At MB factor 15, groups of 15 collapsed readout rows are being reconstructed sequentially in our current implementation. As each collapsed group is independent of the others, the reconstruction is highly parallelizable, and is warranted to yield significant speed-up when parallel processing is

enabled in C/C++ environment. Berkeley Advanced Reconstruction Toolbox (BART) (56) is a library for efficient image reconstruction, and is likely to provide significant time savings during computation. As ESPIRiT coil sensitivity estimation is included in the BART package, migrating Wave-CAIPI to this platform may enable rapid coil profile estimation and parallel imaging reconstruction, thus facilitating near real-time reconstruction for clinical applications.

Lastly, the 1-mm isotropic data were acquired in 70 s using a prototype SMS-RARE sequence, where echo spacing and gradient timing have not been fully optimized. With additional engineering, we expect that this 1-mm isotropic acquisition can be completed in just 1 min.

#### CONCLUSIONS

In this work we combine the recently developed Multi-PINS refocusing pulses with the novel Wave-CAIPI controlled aliasing strategy and SMS acceleration to achieve dramatic speed-up of RARE/TSE imaging. While Multi-PINS pulses allow simultaneous refocusing of large number of slices with reduced SAR and peak RF power deposition, Wave-CAIPI substantially reduces the g-factor penalty during SMS reconstruction thanks to improved usage of 3D coil sensitivity information. The integration of these techniques permits 1 mm isotropic RARE/TSE imaging with whole brain coverage in 70 s, for conventional contrast and ETL RARE/TSE acquisitions, while incurring maximum and average g-factors of  $g_{\max} = 1.34$  and  $g_{\text{avg}} = 1.12$  at effective MB factor 13. This work has the potential to be highly impactful to clinical brain MRI examinations, which heavily relies on RARE based imaging. Such technology could be used to dramatically shorten clinical brain exams, and thus increase patient throughput, cost efficiency, and compliance in general. It would improve the diagnostic power of MRI while expanding its feasibility and availability in time-sensitive situations such as acute stroke.

#### REFERENCES

- Hennig J, Nauerth A, Friedburg H. RARE imaging: a fast imaging method for clinical MR. *Magn Reson Med* 1986;3:823–833.
- Hennig J. Multiecho imaging sequences with low refocusing flip angles. *J Magn Reson* 1988;78:397–407.
- Hennig J, Weigel M, Scheffler K. Multiecho sequences with variable refocusing flip angles: optimization of signal behavior using smooth transitions between pseudo steady states (TRAPS). *Magn Reson Med* 2003;49:527–535.
- Breuer F, Blaimer M, Heidemann RM, Mueller MF, Griswold MA, Jakob PM. Controlled aliasing in parallel imaging results in higher acceleration (CAIPIRINHA) for multi-slice imaging. *Magn Reson Med* 2005;53:684–691.
- Feinberg D, Moeller S, Smith S, Auerbach E, Ramanna S, Glasser MF, Miller K, Ugurbil K, Yacoub E. Multiplexed echo planar imaging for sub-second whole brain fMRI and fast diffusion imaging. *PLoS One* 2010;5:e15710.
- Moeller S, Yacoub E, Olman CA, Auerbach E, Strupp J, Harel N, Ugurbil K. Multiband multislice GE-EPI at 7 tesla, with 16-fold acceleration using partial parallel imaging with application to high spatial and temporal whole-brain fMRI. *Magn Reson Med* 2010;63:1144–1153.
- Setsoompop K, Gagoski B, Polimeni JR, Witzel T, Wedeen VJ, Wald LL. Blipped-controlled aliasing in parallel imaging for simultaneous multislice echo planar imaging with reduced g-factor penalty. *Magn Reson Med* 2012;67:1210–1224.

8. Feinberg D, Setsompop K. Ultra-fast MRI of the human brain with simultaneous multi-slice imaging. *J Magn Reson* 2013;229:90–100.
9. Larkman D, Hajnal J, Herlihy AH, Coutts GA, Young IR, Ehnholm G. Use of multicoil arrays for separation of signal from multiple slices simultaneously excited. *J Magn Reson Imaging* 2001;13:313–317.
10. Müller S. Multifrequency selective rf pulses for multislice MR imaging. *Magn Reson Med* 1988;6:364–371.
11. Norris D, Koopmans PJ, Boyacıoğlu R, Barth M. Power independent of number of slices (PINS) radiofrequency pulses for low-power simultaneous multislice excitation. *Magn Reson Med* 2011;66:1234–1240.
12. Eichner C, Setsompop K, Koopmans P, Lutzkendorf R, Norris D, Turner R, Wald L, Heidemann RM. Slice accelerated diffusion-weighted imaging at ultra-high field strength. *Magn Reson Med* 2014;71:1518–1525.
13. Koopmans P, Boyacıoğlu R, Barth M, Norris D. Whole brain, high resolution spin-echo resting state fMRI using PINS multiplexing at 7T. *Neuroimage* 2012;62:1939–1946.
14. Norris D, Boyacıoğlu R, Schulz J, Barth M, Koopmans PJ. Application of PINS radiofrequency pulses to reduce power deposition in RARE/turbo spin echo imaging of the human head. *Magn Reson Med* 2014;71:44–49.
15. Eichner C, Wald LL, Setsompop K. A low power radiofrequency pulse for simultaneous multislice excitation and refocusing. *Magn Reson Med* 2014;72:949–958.
16. Bilgic B, Gagoski B, Cauley S, Fan AP, Polimeni J, Grant P, Wald L, Setsompop K. Wave-CAIPI for highly accelerated 3D imaging. *Magn Reson Med* 2014. doi: 10.1002/mrm.25347.
17. Souza S, Szumowski J. SIMA: simultaneous multislice acquisition of MR images by Hadamard-encoded excitation. *J Comput Assist Tomogr* 1988;12:1026–1030.
18. Wong E. Optimized phase schedules for minimizing peak RF power in simultaneous multi-slice RF excitation pulses. In Proceedings of the 20th Annual Meeting of ISMRM, Melbourne, Australia, 2012. Abstract 2209.
19. Auerbach EJ, Xu J, Yacoub E, Moeller S, Uğurbil K. Multiband accelerated spin-echo echo planar imaging with reduced peak RF power using time-shifted RF pulses. *Magn Reson Med* 2013;69:1261–1267.
20. Conolly S, Nishimura D, Mackovski A, Glover G. Variable-rate selective excitation. *J Magn Reson* 1988;78:440–458.
21. Breuer F, Blaimer M, Mueller MF, Seiberlich N, Heidemann RM, Griswold MA, Jakob PM. Controlled aliasing in volumetric parallel imaging (2D CAIPIRINHA). *Magn Reson Med* 2006;55.3:549–556.
22. Ståb D, Ritter C, Breuer F, Weng AM, Hahn D, Köstler H. CAIPIRINHA accelerated SSFP imaging. *Magn Reson Med* 2011;65:157–164.
23. Setsompop K, Cohen-Adad J, Gagoski B, Raji T, Yendiki A, Keil B, Wedeen VJ, Wald LL. Improving diffusion MRI using simultaneous multi-slice echo planar imaging. *Neuroimage* 2012;63:569–580.
24. Feinberg D, Beckett A, Chen L. Arterial spin labeling with simultaneous multi-slice echo planar imaging. *Magn Reson Med* 2013;70:1500–1506.
25. Kim T, Shin W, Zhao T. Whole brain perfusion measurements using arterial spin labeling with multiband acquisition. *Magn Reson Med* 2013;70:1653–1661.
26. Eichner C, Jafari-Khouzani K, Cauley S, et al. Slice accelerated gradient-echo spin-echo dynamic susceptibility contrast imaging with blipped CAIPI for increased slice coverage. *Magn Reson Med* 2013;72:770–778.
27. Uğurbil K, Xu J, Auerbach E, et al. Pushing spatial and temporal resolution for functional and diffusion MRI in the Human Connectome Project. *Neuroimage* 2013;80:80–104.
28. Wright K, Harrell M, Jesberger J, Landers L, Nakamoto D, Thomas S, Nickel D, Kroeker R, Griswold M, Gulani V. Clinical evaluation of CAIPIRINHA: comparison against a GRAPPA standard. *J Magn Reson Imaging* 2014;39:189–194.
29. Yu M, Lee J, Yoon J, Keifer B, Han J, Choi B. Clinical application of controlled aliasing in parallel imaging results in a higher acceleration (CAIPIRINHA)-volumetric interpolated breathhold (VIBE) sequence for gadoteric acid-enhanced liver MR imaging. *J Magn Reson Imaging* 2013;38:1020–1026.
30. Zahneisen B, Poser BA, Ernst T, Stenger VA. Three-dimensional Fourier encoding of simultaneously excited slices: generalized acquisition and reconstruction framework. *Magn Reson Med* 2014;71:2071–2081.
31. Zhu K, Kerr A, Pauly J. Autocalibrating CAIPIRINHA: reformulating CAIPIRINHA as a 3D problem. In Proceedings of the 20th Annual Meeting of ISMRM, Melbourne, Australia, 2012. Abstract 518.
32. Moriguchi H, Duerk J. Bunched phase encoding (BPE): a new fast data acquisition method in MRI. *Magn Reson Med* 2006;55.3:633–648.
33. Breuer F, Moriguchi H, Seiberlich N, Blaimer M, Jakob PM, Duerk JL, Griswold MA. Zigzag sampling for improved parallel imaging. *Magn Reson Med* 2008;60.2:474–478.
34. Seiberlich N, Breuer F, Ehse P, Moriguchi H, Blaimer M, Peter M, Jakob A, Griswold MA. Using the GRAPPA operator and the generalized sampling theorem to reconstruct undersampled non-Cartesian data. *Magn Reson Med* 2009;61.3:705–715.
35. Feinberg D, Oshio K. GRASE (gradient-and spin-echo) MR imaging: a new fast clinical imaging technique. *Radiology* 1991;181:597–602.
36. Oshio K, Feinberg D. GRASE (Gradient-and Spin-Echo) imaging: a novel fast MRI technique. *Magn Reson Med* 1991;20:344–349.
37. Oshio K. vGRASE: separating phase and T2 modulations in 2D. *Magn Reson Med* 2000;44:383–386.
38. Griswold M, Jakob P, Heidemann RM, Nittka M, Jellus V, Wang J, Kiefer B, Haase A. Generalized autocalibrating partially parallel acquisitions (GRAPPA). *Magn Reson Imaging* 2002;47:1202–1210.
39. Ying L, Sheng J. Joint image reconstruction and sensitivity estimation in SENSE (JSENSE). *Magn Reson Med* 2007;57:1196–1202.
40. Pruessmann K, Weiger M, Scheidegger MB, Boesiger P. SENSE: sensitivity encoding for fast MRI. *Magn Reson Med* 1999;42:952–962.
41. Pruessmann K, Weiger M, Börner P, Boesiger P. Advances in sensitivity encoding with arbitrary k-space trajectories. *Magn Reson Med* 2001;46:638–651.
42. Keil B, Wald L. Massively parallel MRI detector arrays. *J Magn Reson* 2013;229:75–89.
43. Wiesinger F, Zanche N De, Pruessmann K. Approaching ultimate SNR with finite coil arrays. In Proceedings of the 13th Annual Meeting of ISMRM, Miami, Florida, USA, 2005. Abstract 672.
44. Mugler J, Brookeman J. Three-dimensional magnetization-prepared rapid gradient-echo imaging (3D MP RAGE). *Magn Reson Med* 1990;15:152–157.
45. De Coene B, Hajnal J, Gatehouse P, Longmore D, White S, Oatridge A, Pennock J, Young I, Bydder G. MR of the brain using fluid-attenuated inversion recovery (FLAIR) pulse sequences. *AJNR Am J Neuroradiol* 1992;13:1555–1564.
46. Liang D, Liu B, Wang J, Ying L. Accelerating SENSE using compressed sensing. *Magn Reson Med* 2009;62.6:1574–1584.
47. Lustig M, Pauly J. SPIRiT: iterative self consistent parallel imaging reconstruction from arbitrary k space. *Magn Reson Med* 2010;64.2:457–471.
48. Cauley S, Xi Y, Bilgic B, Xia J, Adalsteinsson E, Balakrishnan V, Wald LL, Setsompop K. Fast reconstruction for multichannel compressed sensing using a hierarchically semiseparable solver. *Magn Reson Med* 2014. doi: 10.1002/mrm.25222.
49. Otazo R, Kim D, Axel J, Sodickson DK. Combination of compressed sensing and parallel imaging for highly accelerated first pass cardiac perfusion MRI. *Magn Reson Med* 2010;64.3:767–776.
50. Henkelman R, Stanisz G, Graham S. Magnetization transfer in MRI: a review. *NMR Biomed* 2001;14:57–64.
51. Constable R, Anderson A, Zhong J, Gore J. Factors influencing contrast in fast spin-echo MR imaging. *Magn Reson Imaging* 1992;10:497–511.
52. Haase A, Frahm J, Matthaei D, Hancic W, Merboldt K. FLASH imaging. Rapid NMR imaging using low flip-angle pulses. *J Magn Reson* 1986;67:258–266.
53. Uecker M, Lai P, Murphy M, Virtue P, Elad M, Pauly JM, Vasanawala S, Lustig M. ESPIRiT—an eigenvalue approach to autocalibrating parallel MRI: Where SENSE meets GRAPPA. *Magn Reson Med* 2014;71:990–1001.
54. Uecker M, Hohage T, Block KT, Frahm J. Image reconstruction by regularized nonlinear inversion—joint estimation of coil sensitivities and image content. *Magn Reson Med* 2008;60:674–682.
55. Peeters JM, Fuderer M. SENSE with improved tolerance to inaccuracies in coil sensitivity maps. *Magn Reson Med* 2013;69:1665–1669.
56. Uecker M, Virtue P, Ong F, Murphy M, Alley M, Vasanawala S, Lustig M. Software toolbox and programming library for compressed sensing and parallel imaging. In ISMRM Workshop on Data Sampling and Image Reconstruction, Sedona, 2013.

## SUPPORTING INFORMATION

Additional Supporting Information may be found in the online version of this article.

**SUPPORTING FIG. S1.** SMS Wave-CAIPI reconstruction flowchart. Point spread functions estimated on phantom data are combined with coil sensitivity estimates in decoupled SENSE reconstruction for slice unaliasing.